Experimental study of $\frac{1}{2}^+$ isomers in ^{199,201}At

K. Auranen,[1,*] J. Uusitalo,[1] S. Juutinen,[1] U. Jakobsson,[1] T. Grahn,[1] P. T. Greenlees,[1] K. Hauschild,[2] A. Herzáň,[1] R. Julin,[1]
J. Konki,[1] M. Leino,[1] J. Pakarinen,[1] J. Partanen,[1] P. Peura,[1] P. Rahkila,[1] P. Ruotsalainen,[1] M. Sandzelius,[1] J. Sarén,[1]
C. Scholey,[1] J. Sorri,[1] and S. Stolze[1]

[1]*Department of Physics, University of Jyväskylä, P.O. Box 35, FI-40014 Jyväskylä, Finland*
[2]*CSNSM, IN2P3-CNRS, F-91405 Orsay Campus, France*

Using fusion-evaporation reactions, a gas-filled recoil separator, and recoil-electron and recoil-electron-α tagging techniques, a new isomeric $\frac{1}{2}^+$ state $[T_{1/2} = 45(3)$ ms] in ^{201}At is identified, and an earlier reported corresponding state $[T_{1/2} = 273(9)$ ms] in ^{199}At is confirmed. The $\frac{1}{2}^+$ state is suggested to originate from an intruder $\pi(s_{1/2})^{-1}$ configuration. In addition, nuclear structure of states below and above this $\frac{1}{2}^+$ state are studied in both nuclei. The isomer decays through a cascade of an $E3$ transition followed by a mixed $M1/E2$ transition to the $\frac{9}{2}^-$ ground state, and it is interpreted to be fed from nearly spherical $\frac{3}{2}^+$ and $\frac{5}{2}^+$ states originating from $\pi(d_{3/2})^{-1}$ and $\pi(d_{5/2})^{-1}$ configurations, respectively.

PACS number(s): 23.20.Lv, 23.20.Nx, 23.35.+g, 27.80.+w

I. INTRODUCTION

Exciting a proton from the $s_{1/2}$ orbital across the $Z = 82$ shell gap can create a $\frac{1}{2}^+$ intruder state. Such a state is rather well established throughout the bismuth isotopes. The energy of the state decreases as the neutron number decreases, and it becomes the ground state in ^{185}Bi (Ref. [1] and references therein). In odd-mass astatine nuclei the corresponding state was first observed in ^{197}At [2], and it becomes the ground state in ^{195}At [3]. It is also observed to be the ground state in ^{191,193}At [4]. A recent study by Jakobsson *et al.* [5] reports the existence of such a state in ^{199}At. In francium nuclei the $\frac{1}{2}^+$ state has been studied in the isotopes ^{201}Fr [6], ^{203}Fr [5,6], and ^{205}Fr [7]. In ^{199}Fr it most likely becomes the ground state [6,8,9].

For the first time we have observed the intruder $\frac{1}{2}^+$ state in ^{201}At, and we have also confirmed and improved earlier knowledge of the corresponding state in ^{199}At. In this article deexcitation, half-lives, and the level structures above these states are presented.

II. EXPERIMENTAL DETAILS

The experiment was performed in the Accelerator Laboratory at the Department of Physics at the University of Jyväskylä. The astatine nuclei of interest were produced using the fusion evaporation reactions ^{165}Ho(^{40}Ar,4n)^{201}At and ^{165}Ho(^{40}Ar,6n)^{199}At. Relative production yields for nuclei under interest can be seen from the α-particle energy spectra shown in Fig. 1. The holmium target was self-supporting, with a thickness of 350 μg/cm^2. A reset foil made of carbon was placed downstream from the target. Reset-foil thicknesses of 44 and 80 μg/cm^2 were used for ^{201}At and ^{199}At, respectively.

The ^{40}Ar^{8+} beam was produced using an electron cyclotron resonance ion source and accelerated with the K-130 cyclotron. Beam energies of 172 and 205 MeV, typical intensities of 11 and 9 pnA (particle nA), and irradiation times of 83 and 130 h were used for the production of ^{201}At and ^{199}At, respectively.

The JUROGAM2 array of Compton-suppressed high-purity germanium (HPGe) detectors was used to detect prompt γ rays at the target position. The array consists of 24 Clover [10] and all together 15 Phase1 [11] and GASP [12] type detectors. The gas-filled recoil separator RITU [13,14] was used to separate the fusion-evaporation residues (later recoils) from the primary beam and other unwanted particles. The recoils were then transported through a multiwire proportional gas counter (MWPC) to the focal plane of the RITU, where they were studied using the GREAT [15] spectrometer. In GREAT the recoils were implanted into a 300-μm thick double-sided silicon strip detector (DSSD) surrounded by 28 silicon PIN diodes in a box arrangement. At the focal plane γ rays were detected with three Clover and one planar-type HPGe detectors placed in close geometry around the DSSD. The horizontal strips in the DSSD were set to measure recoil and α-particle energies, and the vertical strips were set to measure conversion-electron energies. It is worth noting, that due to the implantation of the recoils, the DSSD works as a calorimetric detector. Therefore the observed K-conversion electron energies are $\sim$12 keV higher in energy than the actual K-conversion electron energy due to the relaxation (Auger electrons, low-energy x rays) of the electron cloud. Due to the same reason the measured $L + M + \cdots$-conversion electron energies correspond to the full transition energy. The horizontal strips in the DSSD were calibrated using known produced α activities, and all the other detectors were calibrated using external sources. Data from all channels were recorded independently using the triggerless total data readout (TDR) [16] method. Absolute time stamps for each event were given by a 100-MHz clock. The data analysis was performed using GRAIN [17] software.
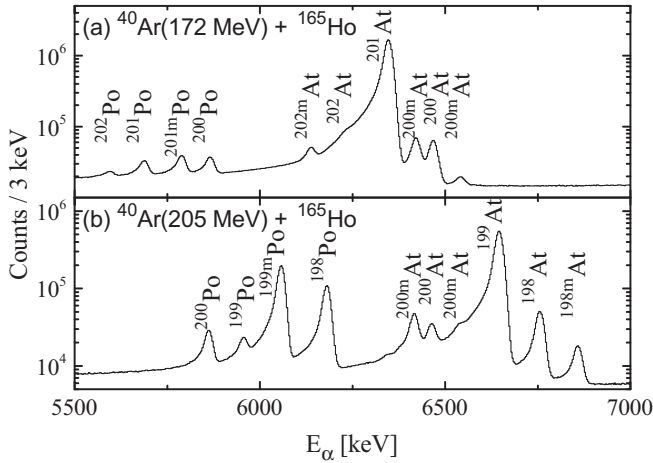
*kalle.auranen@jyu.fi

024310-1

FIG. 1. Raw α-particle energy spectra in DSSD obtained with the reactions used in these studies.

III. RESULTS

A. $\frac{1}{2}^+$ isomer in ^{201}At

The analysis of the ^{201}At data was based on a search for recoil-conversion electron chains (later R-e^- chains) in the same DSSD pixel within 130 ms from the recoil implantation. This is roughly three times the half-life of the $\frac{1}{2}^+$ isomer. The deduction of the half-life is explained at the end of this section. Despite the fact that ^{201}At is an α-active nucleus, the recoil α-decay tagging technique was not usable due to the long half-life (85.2(16) s, Ref. [18]) of ^{201}At with respect to the recoil implantation rate. However, the lack of α-decay tagging was not crucial due to the dominance of the ^{201}At (4n) evaporation channel. The identification of the recoil was based on the time-of-flight between the MWPC and the DSSD, and the energy loss of the recoil in the MWPC.

The energy spectrum of γ rays observed at the focal plane in prompt coincidence with the R-e^- chain electrons, shows two interesting γ-ray peaks. The energies of these are 190.1(1) and 269.1(1) keV, and the spectrum is shown in Fig. 2(a). Electron energy spectra of those R-e^- chains where the electron is in prompt coincidence with either one of these γ rays are shown in Figs. 2(b) and 2(c). The two peaks in these figures represent the K- and $L + M + \cdots$ internal conversions of the 190- and 269-keV transitions. For the 269-keV transition the measured internal-conversion ratio $K/L + M + \cdots = 0.24(1)$ indicates an $E3$ transition because the theoretical [19] ratio is 0.227(5). For the 190-keV transition the corresponding ratio is 3.1(2), and the theoretical ratios are 4.27(9) and 0.45(2) for the $M1$ and $E2$ transitions, respectively. In addition, the 190-keV transition is in coincidence with the 269-keV transition. Based on these arguments, the 190-keV transition is suggested to have a mixed $M1/E2$ character. Based on these observations the spin and parity of the isomer is suggested to be $\frac{1}{2}^+$, and the state between the $\frac{9}{2}^-$ ground state and the isomer is suggested to have a spin and parity of $\frac{7}{2}^-$.
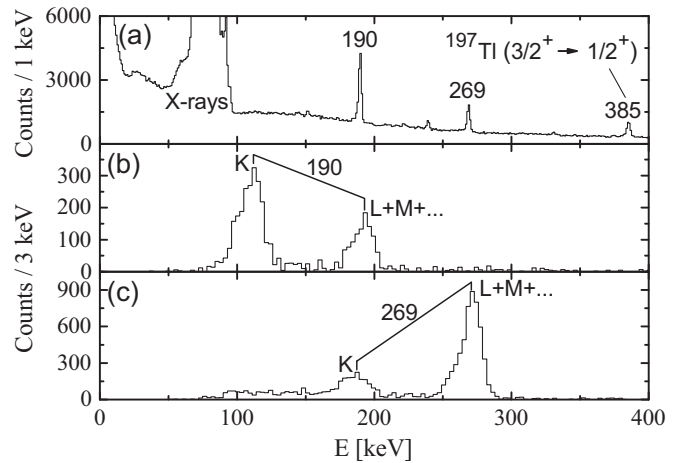

FIG. 2. (a) Recoil-electron tagged γ-ray spectrum observed in the planar detector. Conversion-electron spectra: (b) Electron in coincidence with the 269-keV γ ray observed in the planar germanium detector. (c) Same as panel (b), but with the electron in coincidence with the 190-keV γ ray. In panels (b) and (c), background subtraction has been introduced.

Figure 3 shows energy spectra of prompt γ rays observed in the JUROGAM2 array. Panel 3(a) shows recoil tagged prompt γ rays. In Fig. 3(b) is the R-e^- tagged prompt γ-ray energy spectrum where the electron is in coincidence with the 190- or 269-keV γ ray observed at the focal plane. The spectrum reveals two interesting transitions, with energies of 173 and 433 keV. Because the 173-keV transition has the highest total transition intensity, it is assumed to feed the $\frac{1}{2}^+$ isomer. Figure 3(c) shows an example of the γ-γ analysis of the prompt γ-ray data. Detected γ-ray transitions are shown in Table I together with the angular distribution parameters A_2
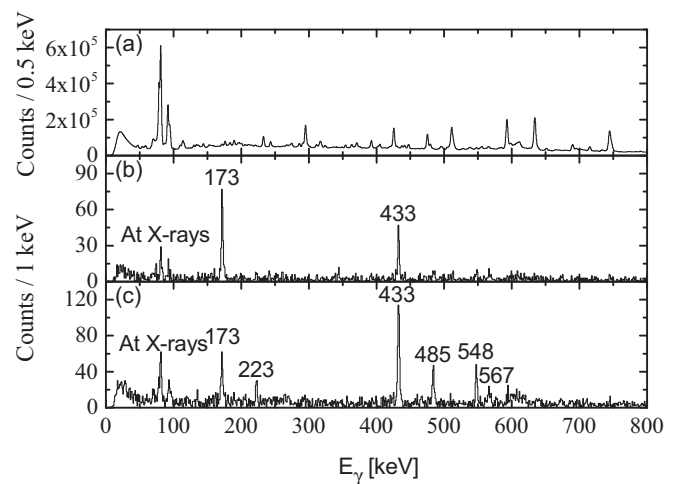

FIG. 3. Prompt γ rays detected in the JUROGAM2 array. (a) Recoil tagged prompt γ rays. (b) R-e^- tagged prompt γ rays, where the electron is in fast coincidence with the 190- or 269-keV delayed γ ray detected in the focal plane Clover array. (c) R-e^- tagged prompt γ rays in fast coincidence with the 173-keV prompt γ ray. In panels (b) and (c), background subtraction has been introduced.

TABLE I. Observed γ rays feeding the $\frac{1}{2}^+$ isomer in ^{201}At. The intensities are from R-e^- tagged singles γ data if not specified.

E_γ (keV)	I_γ (%)	A_2[a]	R[a]	J_i^π	J_f^π
172.6(4)	113(5)[b]		[0.83(5)]	$\frac{3}{2}^+$	$\frac{1}{2}^+$
172.5(4)	18(1)[b]			$\frac{5}{2}^+$	$\frac{3}{2}^+$
223.3(4)	17(1)	$-0.29(7)$	0.74(12)	$\frac{9}{2}^+$	$\frac{7}{2}^+$
242.8(7)	5.7(5)[c]			$\frac{13}{2}^+$	$\frac{11}{2}^+$
433.3(4)	100(4)		1.21(5)	$\frac{7}{2}^+$	$\frac{3}{2}^+$
484.5(4)	41(3)	0.70(6)	1.4(2)	$\frac{9}{2}^+$	$\frac{5}{2}^+$
548.1(4)	48(2)	0.5(2)	1.26(12)	$\frac{11}{2}^+$	$\frac{7}{2}^+$
567.3(4)	37(2)	0.5(3)	1.2(3)	$\frac{13}{2}^+$	$\frac{9}{2}^+$
618.8(6)	7(3)[c]	0.6(4)	1.1(4)	$\frac{15}{2}^+$	$\frac{11}{2}^+$

[a]See Eqs. (1)–(3).

[b]Doublet, intensity from the 173-keV gated, recoil-correlated $\gamma\gamma$ data.

[c]Weak transition, intensity from 173-keV gated, recoil-correlated $\gamma\gamma$ data.

and R, obtained when possible. The angular distribution of γ rays follows the

$$W(\theta) = A_0\{1 + A_2 P_2[\cos(\theta)]\} \qquad (1)$$

distribution function [20], where P_2 is the second-order Legendre polynomial. A positive A_2 value indicates a stretched quadrupole transition and a negative value indicates a stretched dipole transition. In addition to this, the intensity ratios

$$R_1 = \frac{I_\gamma(133.6° + 157.6°)}{I_\gamma(104.5°)} \qquad (2)$$

and

$$R_2 = \frac{I_\gamma(133.6° + 157.6°)}{I_\gamma(75.5°)} \qquad (3)$$

were calculated. The weighted average R of these is shown in Table I. R values of 1.30(7) and 0.70(6) refer to a stretched quadrupole and a stretched dipole transition, respectively [21]. This method was confirmed by comparing measured angular distributions to the multipolarities of previously known transitions [22,23].

The level structure above the $\frac{1}{2}^+$ isomer was constructed based on the γ-γ coincidence information, total transition intensity information, multipolarity information, and energy-sum arguments. The obtained level scheme is shown in Fig. 4. The angular-distribution coefficients for the lower 173-keV transition remain inconclusive. This can be caused by the fact that the spin of the decaying state is rather low and the transition lies low in the cascade. Therefore the initial alignment obtained in the fusion-evaporation reaction is lost. On the other hand, this inconclusiveness might refer to the transition being of a mixed $M1/E2$ character. In addition, in the 548-keV gated γ-γ spectrum the total transition intensities of the lower 173-keV transition and the 433-keV $E2$ transitions must be equal. This suggests that the lower 173-keV transition could be an $E2$ transition, but the x-ray intensity suggests that it
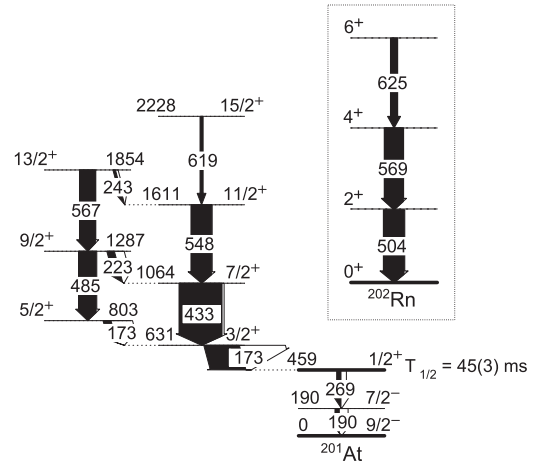

FIG. 4. Level scheme of the $\frac{1}{2}^+$ structure in ^{201}At. The intensities of transitions below the $\frac{1}{2}^+$ state and the lower 173-keV transition are not to scale. For the inset, see Sec. IV.

cannot be a pure $E2$-type transition. Based on these arguments the transition is assigned to be a mixed $M1/E2$-type transition.

Figure 5 shows the time distribution between the recoil implantation into the DSSD and the subsequent (conversion) electron. In this case the 130-ms time gate was omitted. As one can see from Fig. 5(a), the $\beta+$/EC background is dominating the distribution. Therefore the conversion electron was identified by demanding a coincidence between the electron and the 190- or 269-keV γ ray below the $\frac{1}{2}^+$ isomer [Fig. 5(b)]. In addition, the recoil was identified by demanding a prompt 173- or 433-keV γ ray to be observed
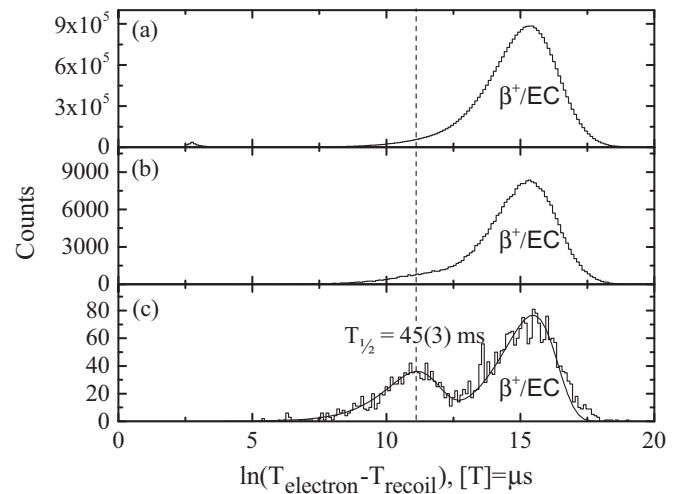

FIG. 5. Logarithm of the time difference between the recoil implantation and the observation of the following electron in the same pixel of the DSSD. (a) All observed recoil-electron chains. (b) Electrons in coincidence with the 190- or 269-keV γ ray observed at the focal plane. (c) Same as panel (b), but the recoil is correlated with the 173- or 433-keV prompt γ ray observed in the JUROGAM2 array. The half-life of the $\frac{1}{2}^+$ state of 45(3) ms was obtained using the logarithmic time-scale method [24].

in the JUROGAM2 array. These two requirements reduced the background significantly, and as a result [Fig. 5(c)] a two-peak distribution with well-separated $\frac{1}{2}^+$ activity with some remaining $\beta+$/EC background is extracted. Fitting a two-component function [24] to these peaks gives the half-life of the $\frac{1}{2}^+$ isomer to be 45(3) ms.

B. $\frac{1}{2}^+$ isomer in ^{199}At

The search for the $\frac{1}{2}^+$ isomer in ^{199}At was based on searching for recoil-conversion electron-^{199}At α particle chains (later R-e^--^{199}At α chain) in the same DSSD pixel within time conditions approximately three times the half-life of the activity of interest. Because the estimated half-life for the $\frac{1}{2}^+$ isomer is 310(80) ms [5] the maximum search time between the recoil and the subsequent conversion electron was set to 1 s. The half-life of the ^{199}At ground state is 7.03(15) s [25]; thus the maximum search time between the conversion electron and the subsequent α particle was set to 21 s.

The $\frac{1}{2}^+$ isomer is known to deexcite through a ∼90-keV $E3$ transition [5]. Figure 6(a) shows the R-e^--^{199}At α tagged conversion-electron energy spectrum. The lower-energy 103(2)-keV peak corresponds to the $L + M + \cdots$ internal-conversion transition of the $\frac{1}{2}^+$ isomer. Due to the low transition energy the K conversion is weak [19]. The peak at ∼160 keV is a sum of the 103-keV electrons and the K-conversion electron from a 141-keV transition below the 103-keV transition. In coincidence with the R-e^--^{199}At α-chain electron there is a 141.0(1)-keV γ ray observed in the planar detector [Fig. 6(b)]. The K conversion of the 141-keV transition is rarely observed alone, because of the strong $L + M + \cdots$ conversion ($\alpha_{L+M\cdots} = 180(15)$, Ref. [19]) of the preceding 103-keV transition. Because of the high x-ray yield the 141-keV transition is suggested to be $M1$ type. In addition,
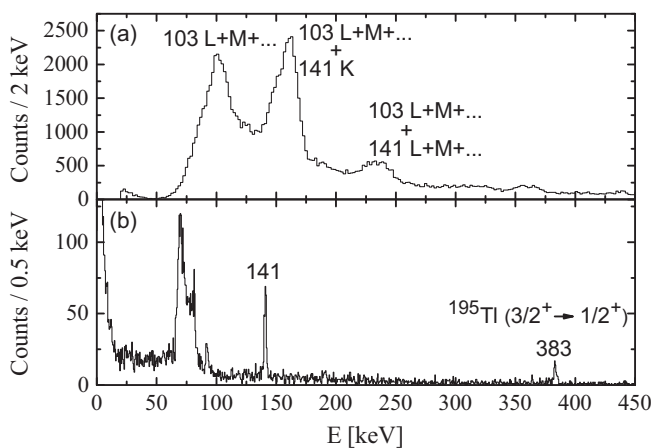
TABLE II. Observed γ rays above the $\frac{1}{2}^+$ isomer in ^{199}At. If not specified, values obtained from R-e^--^{199}At α tagged singles data.

E_γ (keV)	I_γ (%)	A_2[a]	R[a]	I_i^π	I_f^π
156.1(4)	100(6)		[0.8(2)][b]	$\frac{3}{2}^+$	$\frac{1}{2}^+$
179.0(5)	17(4)		0.82(14)	$\frac{5}{2}^+$	$\frac{3}{2}^+$
410.2(4)	124(6)	0.05(3)	1.24(8)	$\frac{7}{2}^+$	$\frac{3}{2}^+$
469.4(4)	44(3)		1.8(7)[c]		
526.0(4)	67(4)		1.31(13)	$\frac{11}{2}^+$	$\frac{7}{2}^+$

[a]See Eqs. (1)–(3).
[b]R value obtained from $\gamma\gamma$ data using sum gate over all other transitions.
[c]R value obtained from 156-keV gated $\gamma\gamma$ data.

the half-life of the isomer, lack of x-rays in coincidence with the 141-keV transition, and the systematics in this part of the nuclide chart all indicate that the 103-keV transition type is $E3$. Just like in the ^{201}At case, the spin and parity of the isomer is suggested to be $\frac{1}{2}^+$, and the state between the $\frac{9}{2}^-$ ground state and the isomer is suggested to be $\frac{7}{2}^-$.

Figure 1(b) shows the α-particle energy spectrum measured in this experiment. One of the side products in the ^{199}At experiment was ^{200m}At, with a well-known 10^- isomer reported by Huyse *et al.* [26]. This isomer dacays mainly through internal 231-keV $E3$ transition ($b(E3) = 89.5(3)$ %), but the population of this state is weak. However, it may contribute through random coincidences with the ^{199}At α-particles. This overlaps with the sum-peak of $L + M + \cdots$ conversions of the 103- and 141-keV transitions at ∼235 keV.

The observed γ-ray transitions above the $\frac{1}{2}^+$ isomer are listed in Table II. The type of the 156-keV transition is assigned to be mixed $M1$/$E2$ for the same reasons as in the case of the lower 173-keV transition in ^{201}At. Figure 7(a) shows the
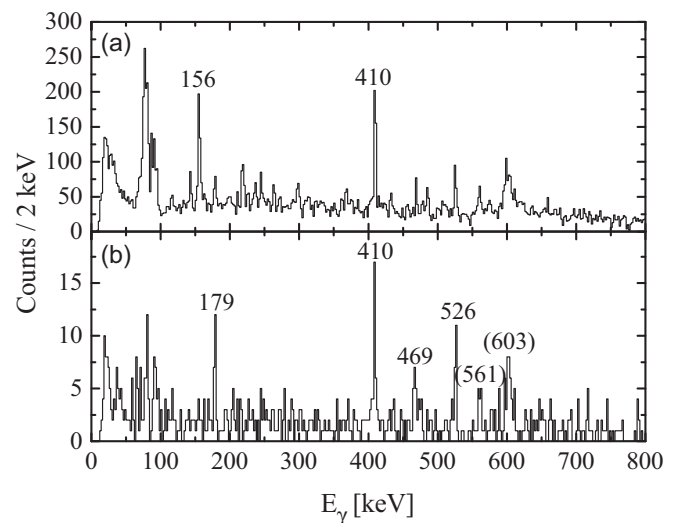

FIG. 6. (a) Conversion-electron energy spectrum related to R-e^--^{199}At α chains. The lowest energy electron peak corresponds to the $L + M + \cdots$-converted transition of the $\frac{1}{2}^+$ isomer. The peak at ∼160 keV corresponds to the sum of the previous transition and the K-conversion of the subsequent 141-keV transition. (b) γ rays in coincidence with the 103-keV conversion electron observed using the planar detector.

FIG. 7. R-e^--^{199}At α tagged energy spectrum of prompt γ rays detected in the JUROGAM2 array. (a) Electron energy of 163 keV demanded. (b) γ rays in coincidence with the 156-keV prompt γ ray with background reduction. Transitions in brackets most likely belong to ^{199}At Band 1 [27] or ^{199}Po [25].
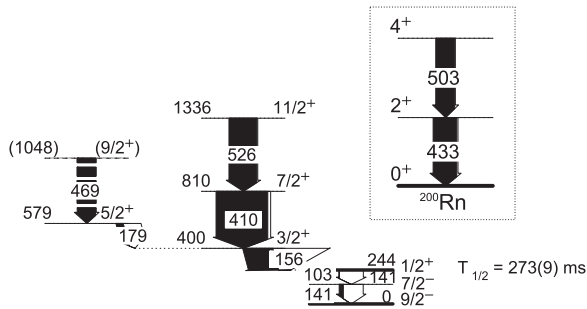
FIG. 8. Level scheme of the $\frac{1}{2}^+$ structure in ^{199}At. The intensity of the 156-keV transition and the transitions below the $\frac{1}{2}^+$ state are not to scale. For the inset, see Sec. IV.

energy spectrum of prompt γ-rays seen in the JUROGAM2 array, where the R-e^--^{199}At α chain with $\sim$160-keV electron energy has been demanded at the focal plane. The spectrum shows two dominating γ-ray peaks with energies of 156 and 410 keV. The γ-ray intensities for these transitions are 100 and 124, respectively, but the 156-keV $M1/E2$ transition has an internal-conversion branch higher than that of the 410-keV $E2$ transition [19]. Therefore the total transition intensity of the 156-keV transition is higher, and it is assumed to feed the $\frac{1}{2}^+$ isomer. Figure 7(b) shows an example of the R-e^--^{199}At α tagged γ-γ analysis. In the example γ rays in coincidence with the 156-keV transition are shown. The level structure feeding the $\frac{1}{2}^+$ isomer was constructed based on the same arguments as in the case of ^{201}At, and the obtained level scheme is shown in Fig. 8. The spin and parity of the state deexciting by the 469-keV γ transition is left tentative, even though the type of this transition is known. Systematics in this area of the nuclide chart suggests that the 469-keV transition should be on top of the 179-keV transition. Due to low statistics in γ-γ data this
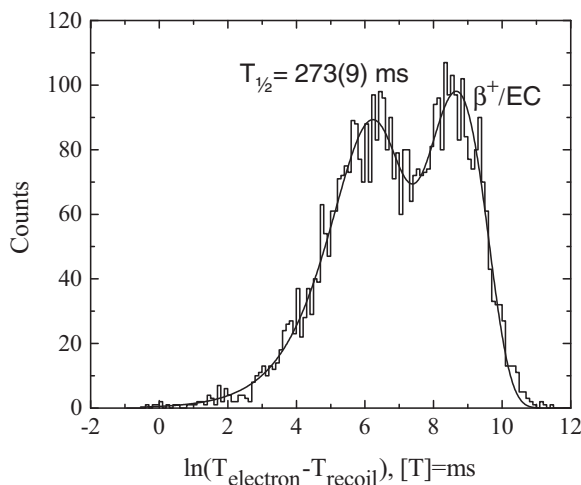

FIG. 9. Logarithm of the time difference between recoil implantation and the observation of the subsequent electron in the same pixel of the DSSD. In addition to the R-e^--^{199}At α chain, the 156- or 410-keV prompt γ ray must be observed in the JUROGAM2 array. In this analysis, the 1-s recoil-electron time gate was omitted. The logarithmic time-scale method [24] yields a half-life of 273(9) ms.

coincidence was not confirmed. The situation is similar to that for the higher 173- and 485-keV transitions in ^{201}At (Fig. 4).

The half-life of 273(9) ms for the $\frac{1}{2}^+$ isomer in ^{199}At was extracted in a way similar to that used in the case of ^{201}At (Fig. 9).

IV. DISCUSSION

We have studied the structures above and below the isomeric intruder $\frac{1}{2}^+$ states in ^{199,201}At. The results for ^{199}At are in agreement with our earlier result [5], based on lower statistics. The extracted half-life 273(9) ms matches well with the previous result 310(80) ms, and hence the extracted transition strength of the $E3$ transition 0.09(2) W.u. is also consistent. A branch of $\sim$1% was predicted [5] for the α decay of the $\frac{1}{2}^+$ state assuming an unhindered α decay. However, in the present work we could not observe this α decay. The $\frac{1}{2}^+$ state in ^{201}At is reported here for the first time, and the results fit well to the systematics. Also the measured transition strength 0.050(3) W.u. for the $E3$ transition from the $\frac{1}{2}^+$ state in ^{201}At is in accordance with the corresponding values in neighboring nuclei: 0.09 W.u. (^{199}At) and 0.07 W.u. (^{195}At, Ref. [28]).

Figure 10 shows the behavior of the energy of the $\frac{1}{2}^+$ state as a function of neutron number in odd-Z nuclei close to lead. It is evident that the energy of the $\frac{1}{2}^+$ state is pushed down as the neutron number decreases. This behavior is typical for intruder states in this region of the nuclide chart. These $\frac{1}{2}^+$ states are known to originate from the $\pi(s_{1/2})^{-1}$ configuration (see references in Fig. 10). The results from this experiment are coherent when compared to neighboring nuclei. Based on this similarity, we propose that the $\frac{1}{2}^+$ state in ^{199,201}At originates from the $\pi(s_{1/2})^{-1}$ configuration. For comparison, Fig. 10 shows also the level energies of the intruder $\frac{9}{2}^-$ states in Tl isotopes. These states originate from the particle configuration $\pi(h_{9/2})$, but the excitation mechanism is the same as for the $\frac{1}{2}^+$ states in Bi, At, and Fr nuclei. The $\frac{9}{2}^-$ state seems to follow the behavior of the $\frac{1}{2}^+$ state in bismuth nuclei when $N \geqslant 108$, but in lighter Tl isotopes the agreement vanishes.

We have observed a low-lying $\frac{7}{2}^-$ state below the $\frac{1}{2}^+$ isomer in ^{199,201}At. Total Routhian surface calculations presented in Ref. [32] show a sharp change in the ground-state β_2 value between ^{195}At and ^{197}At. In lighter At isotopes the nucleus has an oblate shape, and the odd proton occupies the $\frac{7}{2}^-$[514] Nilsson orbital. This is supported by the observation of low-lying $\frac{7}{2}^-$ states in ^{191,193,195}At originating from the $\frac{7}{2}^-$[514] orbital ([3,4]). However, in ^{199,201}At the ground state $\pi(h_{9/2})$ remains nearly spherical, and therefore the $\frac{7}{2}^-$ state most likely originates from the odd proton in the $\pi(f_{7/2})$ orbital, as it is suggested to do in ^{203,205}Fr [5,7]. This is also supported by the fact that the alternative $\frac{7}{2}^-$ state [$\pi(h_{9/2}) \otimes 2^+$] should lie closer to the $\frac{13}{2}^-$ state which is known to lie at 600 keV [27] and 635 keV [23] in ^{199,201}At, respectively.

In both nuclei there is a low-energy $M1/E2$ transition feeding the isomer. The energies of these transitions are too small to form a rotational cascade with the transitions
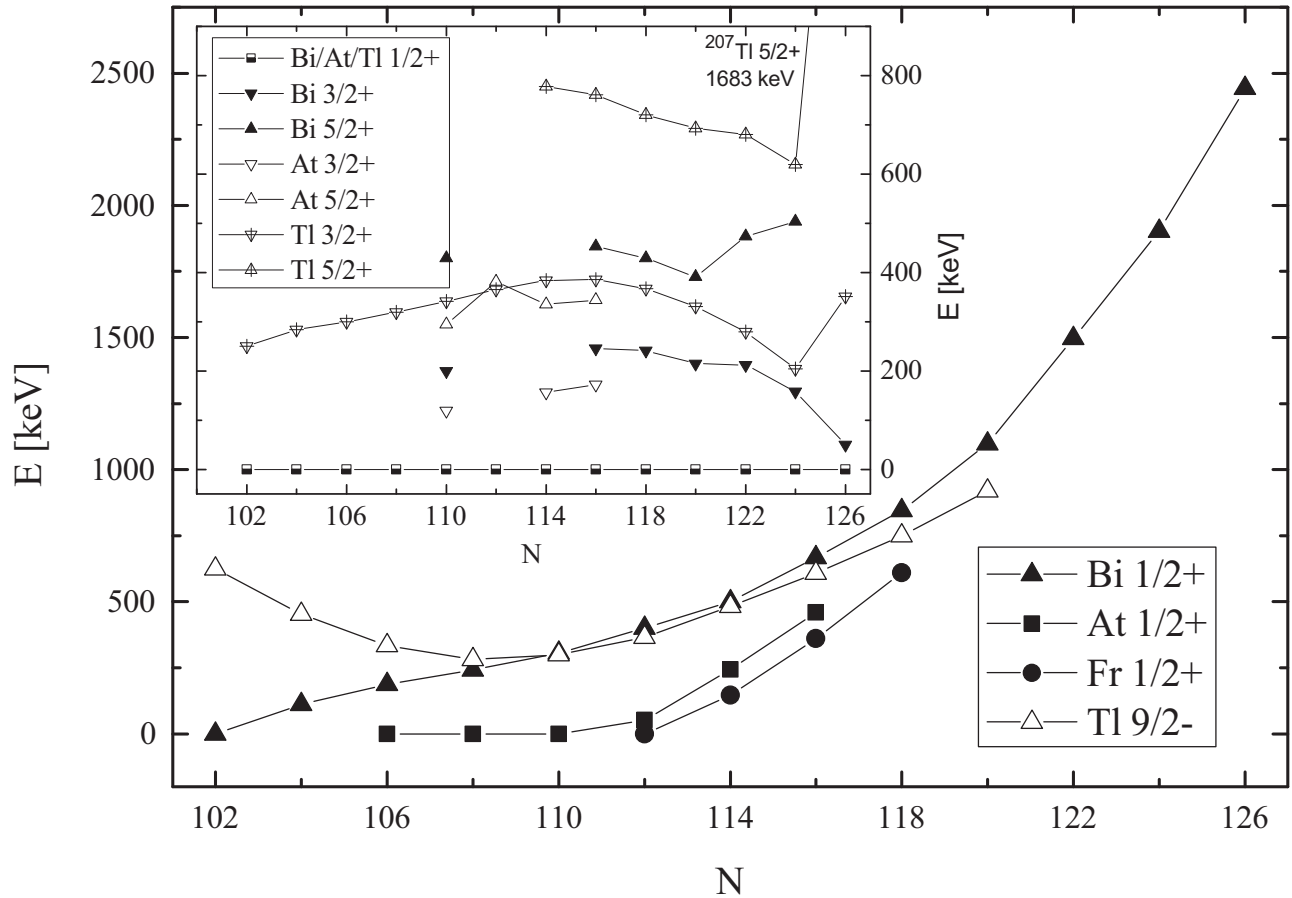
FIG. 10. Energy systematics of the $\frac{1}{2}^+$ isomer originating from the $\pi(s_{1/2})^{-1}$ configuration in nuclei close to magic number $Z = 82$. For comparison, also the behavior of $\frac{9}{2}^-$ states in Tl isotopes originating from the $\pi(h_{9/2})$ structure is shown. The inset shows the level structure feeding the $\frac{1}{2}^+$ state with respect to the $\frac{1}{2}^+$ level energy. Neutron numbers for nuclei studied in this experiment are 114 and 116. Data for Bi isotopes are taken from Refs. [1,4,25,29–31], for At from this work and Refs. [3,4,28,32], for Fr from Refs. [5–7], and for Tl isotopes from Refs. [29,30,33–36].

above them. Therefore, the feeding state most likely has a spin and parity of $\frac{3}{2}^+$, and it is suggested to originate from the $\pi(d_{3/2})^{-1}$ configuration. Similarly the $\frac{5}{2}^+$ state is suggested to originate from the $\pi(d_{5/2})^{-1}$ configuration. This interpretation is supported by the fact that both states follow the systematics of the $\frac{3}{2}^+$ and the $\frac{5}{2}^+$ states in Bi and Tl isotopes. These states have been suggested to originate from the mentioned configurations [29]. The inset in Fig. 10 shows this development as a function of neutron number.

The structure on top of the $\frac{5}{2}^+$ state feeds the structure on top of the $\frac{3}{2}^+$ state through low-energy $M1$ transitions, but not vice versa. This excludes the possibility that two cascades are signature partners from the same rotational structure. In addition, the insets in Figs. 4 and 8 show the lowest excited states in the Rn isotone partners of the studied nuclei. These states show a level pattern with some anharmonics as might be expected when coupling harmonic vibrations to single-particle structures [37]. Transition energies in these structures are very similar to those above the $\frac{3}{2}^+$ and $\frac{5}{2}^+$ states in ^{199,201}At. Based

on these similarities we propose that the $\frac{3}{2}^+$ and $\frac{5}{2}^+$ states are still nearly spherical, and the $\frac{7}{2}^+$, $\frac{11}{2}^+$, $\frac{15}{2}^+$, and $(\frac{9}{2}^+, \frac{13}{2}^+)$ states originate from the proton hole in the $d_{3/2}$ ($d_{5/2}$) orbital coupled to the 2^+, 4^+, and 6^+ states of the Rn core.

Low-lying states in odd-Z nuclei above shell closures are often compared to corresponding states in their lighter even-Z isotones (see, for example, Refs. [5,7,27]). In this case the comparison to the higher-Z radon isotones is reasonable, because the $\frac{1}{2}^+$ state can be described as the creation of a proton hole in the radon core. It is worth noting that the radon isotones are nearly spherical in their ground states [37].

In both nuclei there is a possibility to bypass the $\frac{1}{2}^+$ isomer with a high energy $E1$ transition, for example, from the $\frac{7}{2}^+$ state to the $\frac{9}{2}^-$ ground state. These transitions have not been observed, as they are most likely hindered. This is due to the fact that transitions from positive-parity states above the $\frac{1}{2}^+$ isomer to a negative-parity ground state or the $\frac{7}{2}^-$ state require significant structural changes. In the case of the example transition, this means a transition between states with

a configuration of $\pi(d_{3/2})^{-1} \otimes 2^+$ and $\pi(h_{9/2})$. However there is an alternative, collective decay path inside the vibrational band to the $\pi(d_{3/2})^{-1}$ orbital which dominates.

V. SUMMARY

We have observed very similar properties for the isomeric $\frac{1}{2}^+$ structure in both ^{199}At and ^{201}At. The isomer is suggested to originate from the $\pi(s_{1/2})^{-1}$ configuration. This isomer is fed from nearly spherical $\frac{3}{2}^+$ and $\frac{5}{2}^+$ states originating most likely from $\pi(d_{3/2})^{-1}$ and $\pi(d_{5/2})^{-1}$ configurations, respectively. The isomer decays through a cascade consisting of an $E3$ transition followed by a mixed $M1/E2$ transition to the $\frac{9}{2}^-$ ground state.

The obtained results agree well with our earlier results and the systematics in this region of the nuclear chart.

[1] A. Andreyev *et al.*, Phys. Rev. C **69**, 054308 (2004).

[2] E. Coenen *et al.*, Z. Phys. A **324**, 485 (1986).

[3] H. Kettunen *et al.*, Eur. Phys. A **16**, 457 (2003).

[4] H. Kettunen *et al.*, Eur. Phys. A **17**, 537 (2003).

[5] U. Jakobsson *et al.*, Phys. Rev. C **87**, 054320 (2013).

[6] J. Uusitalo *et al.*, Phys. Rev. C **71**, 024306 (2005).

[7] U. Jakobsson *et al.*, Phys. Rev. C **85**, 014309 (2012).

[8] J. Uusitalo *et al.*, Phys. Rev. C **87**, 064304 (2013).

[9] Z. Kalaninová *et al.*, Phys. Rev. C **87**, 044335 (2013).

[10] G. Duchêne *et al.*, Nucl. Instrum. Methods Phys. Res., Sect. A **432**, 90 (1999).

[11] C. W. Beausang *et al.*, Nucl. Instrum. Methods Phys. Res., Sect. A **313**, 37 (1992).

[12] C. Rossi Alvarez, Nucl. Phys. News **3**, 10 (1993).

[13] J. Sarén *et al.*, Nucl. Instrum. Methods Phys. Res., Sect. A **654**, 508 (2011).

[14] M. Leino *et al.*, Nucl. Instrum. Methods Phys. Res., Sect. B **99**, 653 (1995).

[15] R. D. Page *et al.*, Nucl. Instrum. Methods Phys. Res., Sect. B **204**, 634 (2003).

[16] I. H. Lazarus *et al.*, IEEE Trans. Nucl. Sci. **48**, 567 (2001).

[17] P. Rahkila, Nucl. Instrum. Methods Phys. Res., Sect. A **595**, 637 (2008).

[18] F. G. Kondev, Nucl. Data Sheets **108**, 365 (2007).

[19] T. Kibédi *et al.*, Nucl. Instrum. Methods Phys. Res., Sect. A **589**, 202 (2008).

[20] E. Der Mateosian *et al.*, At. Data Nucl. Data Tables **13**, 391 (1974).

[21] P. Ruotsalainen, Doctoral thesis, JYFL Research Report No. 8/2013 (2013).

[22] K. Auranen *et al.* (unpublished).

[23] K. Dybdal, T. Chapuran, D. B. Fossan, W. F. Piel, D. Horn, and E. K. Warburton, Phys. Rev. C **28**, 1171 (1983).

[24] K. H. Schmidt, Eur. Phys. J. A **8**, 141 (2000).

[25] B. Singh, Nucl. Data Sheets **108**, 79 (2007).

[26] M. Huyse, P. Decrock, P. Dendooven, G. Reusen, P. Van Duppen, and J. Wauters, Phys. Rev. C **46**, 1209 (1992).

[27] U. Jakobsson *et al.*, Phys. Rev. C **82**, 044302 (2010).

[28] M. Nyman *et al.*, Phys. Rev. C **88**, 054320 (2013).

[29] K. Heyde *et al.*, Phys. Rep. **102**, 291 (1983).

[30] E. Coenen, K. Deneffe, M. Huyse, P. Van Duppen, and J. L. Wood, Phys. Rev. Lett. **54**, 1783 (1985).

[31] P. Nieminen *et al.*, Phys. Rev. C **69**, 064326 (2004).

[32] K. Andgren *et al.*, Phys. Rev. C **78**, 044328 (2008).

[33] W. Kratschmer *et al.*, Nucl. Phys. A **201**, 179 (1973).

[34] F. G. Kondev *et al.*, Nucl. Data Sheets **112**, 707 (2011).

[35] G. J. Lane *et al.*, Nucl. Phys. A **586**, 316 (1995).

[36] J. C. Batchelder *et al.*, Eur. Phys. J. A **5**, 49 (1999).

[37] D. J. Dobson *et al.*, Phys. Rev. C **66**, 064321 (2002).